Antiviral Research 222 (2024) 105814

Contents lists available at ScienceDirect

Antiviral Research

journal homepage: www.elsevier.com/locate/antiviral

Generation and evaluation of protease inhibitor-resistant SARS-CoV-2 strains

Hawa Sophia Bouzidi [a,1], Jean-Sélim Driouich [a,1], Raphaëlle Klitting [a,1], Ornéllie Bernadin [a], Géraldine Piorkowski [a], Rayane Amaral [a], Laurent Fraisse [b], Charles E. Mowbray [b], Ivan Scandale [b], Fanny Escudié [b], Eric Chatelain [b], Xavier de Lamballerie [a], Antoine Nougairède [a], Franck Touret [a,*]

[a] Unité des Virus Émergents, UVE: Aix Marseille Univ, IRD 190, INSERM 1207, Marseille, France
[b] Drugs for Neglected Diseases Initiative, Geneva, Switzerland

ARTICLE INFO

Keywords:
COVID-19
SARS-CoV-2
Antiviral therapy
Protease inhibitors
Resistance

ABSTRACT

Since the start of the SARS-CoV-2 pandemic, the search for antiviral therapies has been at the forefront of medical research. To date, the 3CLpro inhibitor nirmatrelvir (Paxlovid®) has shown the best results in clinical trials and the greatest robustness against variants. A second SARS-CoV-2 protease inhibitor, ensitrelvir (Xocova®), has been developed. Ensitrelvir, currently in Phase 3, was approved in Japan under the emergency regulatory approval procedure in November 2022, and is available since March 31, 2023. One of the limitations for the use of antiviral monotherapies is the emergence of resistance mutations. Here, we experimentally generated mutants resistant to nirmatrelvir and ensitrelvir *in vitro* following repeating passages of SARS-CoV-2 in the presence of both antivirals. For both molecules, we demonstrated a loss of sensitivity for resistance mutants *in vitro*. Using a Syrian golden hamster infection model, we showed that the ensitrelvir M49L mutation, in the multi-passage strain, confers a high level of *in vivo* resistance. Finally, we identified a recent increase in the prevalence of M49L-carrying sequences, which appears to be associated with multiple repeated emergence events in Japan and may be related to the use of Xocova® in the country since November 2022. These results highlight the strategic importance of genetic monitoring of circulating SARS-CoV-2 strains to ensure that treatments administered retain their full effectiveness.

1. Introduction

Since the beginning of the SARS-CoV-2 pandemic in 2020, the search for antiviral therapeutics has been a major focus for medical research. As previously observed with Influenza and HIV, effective countermeasures to treat people can be decisive in managing a health crisis. At the start of the pandemic, the repositioning of broad-spectrum antivirals targeting the replication complex raised great expectations (Wang et al., 2020; Williamson et al., 2020), which were dashed by disappointing results in clinical trials (Beigel et al., 2020). Therapeutic antibodies have subsequently demonstrated their usefulness (Pinto et al., 2020; Starr et al., 2021), but failed to overcome the emergence of variants escaping the humoral response (Touret et al., 2023). Ultimately, the best effects in clinical trials (Hammond et al., 2022) and the greatest robustness against variants (Vangeel et al., 2022) were achieved with the protease inhibitor nirmatrelvir (Owen et al., 2021) (PF-07321332, Paxlovid®), targeting the 3CLpro. This inhibitor of the coronavirus protease 3CLpro (PF-00835231) was originally developed against SARS-CoV-1 (Boras et al., 2021). It is also effective against SARS-CoV-2 by preventing the cleavage of the polyproteins PP1a and PP1ab – effectively blocking the generation of the non-structural proteins essential for viral replication (Jin et al., 2020).

The pharmacokinetics (PK) of nirmatrelvir, whose metabolism includes a predominant role for CYP3A4 (Owen et al., 2021), have been improved by the combination with ritonavir used as an exposure booster. However, this combination may complicate the use of nirmatrelvir in certain patients receiving other drugs whose metabolism may also be modified by ritonavir (Hoertel et al., 2022).

* Corresponding author.
E-mail address: franck.touret@univ-amu.fr (F. Touret).
[1] These authors contributed equally to this work.

https://doi.org/10.1016/j.antiviral.2024.105814
Received 28 November 2023; Received in revised form 10 January 2024; Accepted 17 January 2024
Available online 24 January 2024

In the meantime, a second SARS-CoV-2 3CLpro inhibitor named ensitrelvir (S-217622), was developed by the Japanese company Shionogi. The molecule was identified through a combination of virtual and biological screenings followed by optimization using a structure-based drug design strategy (Unoh et al., 2022). It has been proposed for use without an association with ritonavir (Unoh et al., 2022). Following encouraging results in Phase 2 clinical trials, it is now in Phase 3 (Shionogi, 2023; University of Minnesota, 2023). In Japan, however, ensitrelvir (Xocova®), was approved under the emergency regulatory approval procedure in November 2022 and has been available on prescription since March 31, 2023.

Resistance mutations can represent a major limitation to the use of antiviral mono-therapies. Such mutations may naturally be observed in a proportion of circulating strains in the absence of any apparent specific selective pressure (Bloom et al., 2010; Ip et al., 2023; Kawashima et al., 2023) and/or appear in patients in the context of conditions of use associated with sub-optimal efficiency (e.g., during prolonged use in a patient with long lasting viral replication). For instance, the emergence of resistance against antiviral monotherapy has been observed in patients treated with the monoclonal antibody sotrovimab during the Delta wave of SARS-CoV-2 (Rockett et al., 2022).

Here, we experimentally generated nirmatrelvir and ensitrelvir resistance mutants. For both molecules, we demonstrated a loss in sensitivity for the resistance mutants *in vitro*. Using a Syrian golden hamster model of SARS-CoV-2 infection, we showed that the ensitrelvir resistance mutation M49L confers a high level of resistance *in vivo*. Finally, we identified a recent increase in the prevalence of M49L-carrying sequences, that we link to multiple repeated emergence events in Japan, and may be associated with the commercialization of the molecule in the country since April 2023.

2. Materiel and methods

2.1. Experimental model

2.1.1. Cell line

VeroE6/TMPRSS2 cells (ID 100978) were obtained from CFAR and were grown in MEM (Minimal Essential Medium-Life Technologies) with 7 0.5 % heat-inactivated Fetal Calf Serum (FCS; Life Technologies with 1 % penicillin/streptomycin PS, 5000U.mL^{-1} and 5000 µg mL^{-1} respectively (Life Technologies) and supplemented with 1 % non-essential amino acids (Life Technologies) and G-418 (Life Technologies), at 37 °C with 5 % CO_2.

2.1.2. Viral strain

SARS-CoV-2 strain BavPat1 was obtained from Pr. C. Drosten through EVA GLOBAL (https://www.european-virus-archive.com/) and contains the D614G mutation.

2.1.3. Organisms/strains

Three-week-old female Syrian hamsters (*Mesocricetus auratus*) were purchased from Janvier labs. Three-week-old Syrian hamsters (Janvier labs) were maintained in ISOcage P - Bioexclusion System (Techniplast) with unlimited access to water/food and 14 h/10 h light/dark cycle. Animals were monitored and weighed daily throughout the duration of the study to detect the appearance of any clinical signs of illness/suffering.

2.1.4. Antiviral compounds

Remdesivir was purchased from BLDpharm. ensitrelvir and nirmatrelvir were purchased from MedChemexpress.

3. Method details

3.1. RNA extraction and quantification

Viral RNA was extracted from 100 µL of cell supernatant from passages P8 and P16 using a QIAamp Viral RNA kit on the automated QIAcube (Qiagen), following the manufacturer's instructions. Relative quantification of viral RNA was performed using the GoTaq® 1-Step RT-qPCR System kit (Promega). The mixture contained 5 µL of 2× Master Mix, 0.25 µL of each primer (250 nM), 0.07 µL of probe (75 nM), 0.2 µL of GoScript RT Mix and 3.8 µL of extracted nucleic acids. Assays were performed using the QuantStudio 12 K Flex real-time PCR machine (Life technologies) under the following conditions: 50 °C for 15 min, 95 °C for 2 min, followed by 40 cycles of 95 °C for 3 s, 60 °C for 30 s. Data collection took place during the 60 °C step. Synthetic RNA was used to calculate the amount of viral RNA from standard curves.

3.2. EC_{50} determination

One day prior to infection, 5 × 10^4 VeroE6/TMPRSS2 cells per well were seeded in 100 µL assay medium (containing 2.5 % FBS) in 96 well culture plates. The next day, antiviral compounds were added using the D300e dispenser (TECAN) with eight ½ dilutions. Then, 50 µL/well of a virus mix diluted in medium was added to the wells. Each well was inoculated with 100 $TCID_{50}$ of virus which correspond here to a MOI at 0.002 as classically used for SARS-CoV-2 (Touret et al., 2020). Prior to the assay it was verified for each variant that with this MOI, viruses in the cell culture supernatants were harvested during the logarithmic growth phase of viral replication at 48 h post infection (Touret et al., 2019, 2022). Four virus control wells were included within the plate. Quantification of the viral genome by real-time RT-qPCR as previously described (Touret et al., 2020). Nucleic acid from 100 µL of cell supernatant were extracted using QIAamp 96 DNA kit and Qiacube HT robot (both from Qiagen). Viral RNA was quantified by real-time RT-qPCR (GoTaq 1 step RT-qPCR kit, Promega). Quantification was provided by serial dilutions of an appropriate T7-generated synthetic RNA standard. RT-qPCR reactions were performed on QuantStudio 12 K Flex Real-Time PCR System (Applied Biosystems) and analyzed using QuantStudio 12 K Flex Applied Biosystems software v1.2.3. Primers and probe sequences, which target SARS-CoV-2 N gene, were: Fw: 5′-GGCCGCAAATTGCACAAT-3'; Rev: 5′-CCAATGCGCGACATTCC-3'; Probe: 5′-FAM-CCCCAGCGCTTCAGCGTTCT-BHQ1-3'. Viral inhibition was calculated as follow: 100* (quantity mean VC- sample quantity)/quantity mean VC. The 50 % effective concentrations (EC50 compound concentration required to inhibit viral RNA replication by 50 %) were determined using logarithmic interpolation after performing a nonlinear regression (log (inhibitor) vs. response –Variable slope (four parameters)) as previously described (Touret et al., 2019, 2021a, 2022). All data obtained were analyzed using GraphPad Prism 9 software (Graphpad software).

3.3. Viral titration

One day prior to infection, 5 × 10^4 VeroE6 cells per well were seeded in 100 µL assay medium (containing 2.5 % FBS) in 96 well culture plates. Virus titration was performed using 96-well culture plates containing confluent VeroE6 cells inoculated with 150 µL per well of four-fold dilutions of samples (dilution with medium supplemented with 2.5 % FBS) Plates were incubate 6 days (37 °C, 5 % CO2) The absence or presence of cytopathic effect in each well was read. Infectious titers were estimated using the Reed & Muench method (REED and MUENCH, 1938).

3.4. Mutants generation

One day prior to infection, 5 × 10^5 VeroE6/TMPRSS2 cells per well were seeded in 2 mL assay medium (containing 2.5 % FBS) in 12 well culture plates. The EC50s of Nirmatrelvir and Ensitrelvir were

determined as previously described. Once the EC50s of these two molecules had been determined, successive passages of the virus at an MOI of 0.01 with increasing concentrations of these molecules were carried out in triplicate. Two passages at the EC50 concentration, two passages at 2× [EC50], two passages at 4 × [EC_{50}] and ten passages at 8 × [EC_{50}]. A no-molecule control was also run in triplicate. Between each run, the plates were incubated at 37 °C/5 % CO2 for 72 h. We performed extraction with Qiagen's EZ1 automated system and NGS sequencing (Ion Torrent) for passages P8 and P16. We then performed viral production for passage P16. Viral titration by $TCID_{50}$/mL and growth kinetics of all P16 viruses were performed.

3.5. Growth kinetics

One day prior to infection, 5×10^6 VeroE6/TMPRSS2 cells per well were seeded in 3 mL assay medium (containing 2.5 % FBS) in 6 well culture plates. The following day, the wells were infected with each virus with MOI 0.01, in 1 mL of medium (containing 2.5 % FBS), and incubated at 37 °C/5 % Co2 for 2 h. Sampling at 0 h took place before incubation. The experiment was performed in duplicate. After incubation, a wash with HBSS was performed and 3 mL of medium (containing 2.5 % FBS) was added to each well. Samples were taken at 6 h pi, 24 h pi, 30 h pi, 48 h pi, 54 h pi and 72 h pi. They were extracted by Qiacube as described above and qRT performed.

3.6. Animal experiments

In vivo experiments were approved by the local ethical committee (C2EA—14) and the French "Ministère de l'Enseignement Supérieur, de la Recherche et de l'Innovation" (APAFIS#23975). All experiments were conducted in BSL 3 laboratory.

Three-week-old Syrian hamsters (Janvier labs) were maintained in ISOcage P - Bioexclusion System (Techniplast) with unlimited access to water/food and 14 h/10 h light/dark cycle. Animals were monitored and weighed daily throughout the duration of the study to detect the appearance of any clinical signs of illness/suffering. **G**roups of animals were intranasally infected under general anesthesia (isofluorane) with 50 μL containing 2×10^4 TCID50 of virus diluted in 0.9 % sodium chloride solution. Animal were treated via oral route two times a day with 30 or 60 mg/kg of Ensitrelvir suspended in 0.5 % methylcellulose.

Nasal washes were performed under general anesthesia (isoflurane). Blood and organs were collected immediately after euthanasia (cervical dislocation; realized under general anesthesia (isofluorane)).

Nasal washes were performed with 150 μL 0.9 % sodium chloride solution which was transferred into 1.5 mL tubes containing 0.5 mL of 0.9 % sodium chloride solution, then centrifuged at 16,200 g for 10 min and stored at −80 °C. Left pulmonary lobes were washed in 10 mL of 0.9 % sodium chloride solution, blotted with filter paper, weighed and then transferred into 2 mL tubes containing 1 mL of 0.9 % sodium chloride solution and 3 mm glass beads. They were then crushed using a Tissue Lyser machine (Retsch MM400) for 20min at 30 cycles/s and centrifuged 10 min at 16,200 g. Supernatant media were transferred into 1.5 mL tubes, centrifuged 10 min at 16,200 g and stored at −80 °C.

Right apical lobes were collected into 2 mL tubes containing 0.75 mL of Qiazol lysis reagent (Qiagen) and 3 mm glass beads. They were then crushed using a Tissue Lyser machine (Retsch MM400) for 10min at 30 cycles/s and stored at −80 °C.

3.7. Sequence analysis of the full-length genome

200 μL of lung of infectious cell supernatant (virus stock and HAE) was inactivated with an equal volume of VXL lysis buffer (Qiagen) and viral RNA was extracted using an EZ1 Advanced XL robot with the EZ1 mini virus 2.0 kit (both from Qiagen) and linear acrylamide (ThermoFisher Scientific) in place of carrier RNA. The extracts were then subjected to quantitative real-time RT-PCR in order to standardize the amounts of viral RNA used during complete genome amplification (see below).

A specific set of primers (Supplementary table 5) was used to generate thirteen amplicons covering the entire genome with the Superscript IV one step RT-PCR System (ThermoFisher Scientific). PCR mixes (final volume 25 μL) contained 2.5 μL containing a standard quantity of viral RNA from the nucleic acid extract, 0.75 μL of each primer (10 μM), 12.5 μL of 2*X* Platinum SuperFi RT-PCR Master Mix, 8.25 μL of RNA free water and 0.25 μL SuperScript IV RT Mix. Amplifications were performed with the following conditions: 15 s at 55 °C, 2 min at 98 °C, then 40 cycles of 10 s at 98 °C, 10 s à 56 °C and 1.5 min at 72 °C. Size of PCR products was verified by gel electrophoresis. For each sample, an equimolar pool of all amplicons was prepared and purified using Monarch PCR & DNA Cleanup Kit (New England Biolabs). After Qubit quantification using Qubit® dsDNA HS Assay Kit and Qubit 2.0 fluorometer (Thermo Fisher) amplicons were sonicated (Bioruptor®, Diagenode, Liège, Belgium) into 250 pb long fragments. Libraries were built adding to fragmented DNA barcode for sample identification and primers with Ion Plus Fragment Library Kit using AB Library Builder System (Thermo Fisher). To pool equimolarly the barcoded samples, a real time PCR quantification step was performed using Ion Library TaqMan™ Quantitation Kit (Thermo Fisher). Next steps included an emulsion PCR of the pools and loading on 530 chips performed using the automated Ion Chef instrument (Thermo Fisher), followed by sequencing using the S5 Ion torrent technology (Thermo Fisher), following manufacturer's instructions. Consensus sequence was obtained after trimming of reads (reads with quality score <0.99, and length <100 pb were removed and the 30 first and 30 last nucleotides were removed from the reads) and mapping of the reads on a reference (MT594401.1) using CLC genomics workbench software v.21.0.5 (Qiagen). Parameters for reference-based assembly consisted of match score = 1, mismatch cost = 2, length fraction = 0.5, similarity fraction = 0.8, insertion cost = 3, and deletion cost = 3. A de novo contig was also produced to ensure that the consensus sequence was not affected by the reference sequence.

Mutation frequency for each position was calculated as the number of reads with a mutation compared to the consensus sequence divided by the total number of reads at that site.

3.8. Public sequence data analysis

3.8.1. Datasets

We downloaded all three sets of SARS-CoV-2 sequences from the GISAID public database: (1) all sequences (and attached metadata) containing an M to L change at position 49 in the NSP5; (2) all EG.5.1.1 sequences (filtering out low coverage and incomplete sequences) from Japan collected between July and October 2023; (3) all EG.5.1.1 sequences (filtering out low coverage and incomplete sequences) from North America collected between July and October 2023; (4) all sequences (and attached metadata) containing an M to I change at position 49 in the NSP5.

We first removed all sequences with >5 % of ambiguous nucleotides from all datasets except for the one corresponding to EG.5.1.1 M49L sequence. Then, to obtain a computationally tractable dataset for phylogenetic inference, we randomly downsampled the EG.5.1.1 North America dataset (filtering out duplicates) to 500 sequences, and combined it with all EG.5.1.1 sequences from Japan. We added all EG.5.1.1 sequences carrying the M49L mutation. After the first maximum likelihood (ML) inference, we removed three sequences corresponding to extremely long terminal branches (GISAID Accession IDs: 18434659, 18226914, 18432517), yielding a final dataset of 2603 sequences. All GISAID accession numbers are available in Supp. Table 2, the alignment and trees are available at https://github.com/rklitting/SARS-CoV-2-resistance.

3.8.2. Phylogenetic analysis

For the M49L and M49I sequences lineage analysis, we assigned lineages to each of the M49L sequences using the Pangolin lineage assigner (version 4.3) (O'Toole et al., 2021). Classification failed for 3 out of the 267 sequences submitted (See Supp. Table 1).

For phylogenetic inference based on M49L-sequences, we aligned the final EG.5.1.1 dataset to the reference genome WIV04 (GISAID Accession: 402,124) using MAFFTv7 (Katoh and Standley, 2013). To provide some phylogenetic context to the EG.5.1.1 lineage, we added the set of genomes corresponding to WHO reference strains for VOCs, VUIs and VUMs provided by the Los Alamos national laboratory (Korber et al., 2020). Finally, we performed the masking of sites previously identified as potential sequencing errors or suspect homoplasies (Issues with SARS-CoV-2 sequencing data - SARS-CoV-2 coronavirus/nCoV-2019 Genomic Epidemiology, 2020), and removed the 5′ and 3' UTRs. We inferred a first ML phylogeny for this dataset using IQTREE2 under ModelFinder with ultrafast bootstrap approximation (1000 replicates) (Minh et al., 2013, 2020). Finally, we performed 10 ML inference replicates, to control for potential instability in the topology, in particular within the EG.5.1.1 lineage.

3.8.3. Visualizations

The plots were created using matplotlibv3.6.3 (Hunter, 2007)and the tree was visualized using baltic (https://github.com/evogytis/baltic).

4. Results

4.1. Generation of SARS-CoV-2 strains resistant to protease inhibitors

To generate mutants resistant to SARS-CoV-2 protease inhibitors, we first determined the experimental conditions suitable for the emergence of such resistance mutations in cell culture. We evaluated, for both molecules, the half maximal effective concentration EC_{50} in the VeroE6 TMPRSS2 cell line, using remdesivir as a reference compound and the BavPat1 SARS-CoV-2 strain (B.1 lineage carrying the D614G mutation). In line with the literature (Imai et al., 2022; Sasaki et al., 2022; Takashita et al., 2022; Unoh et al., 2022), we obtained EC_{50s} of 0.14 μM and 2.26 μM for ensitrelvir and nirmatrelvir, respectively (Fig. 1a). The EC_{50} of nirmatrelvir appears to be higher than that of ensitrelvir, as we chose to use similar conditions for all our *in vitro* experiments and therefore did not add an efflux pump inhibitor with nirmatrelvir, as other groups may have done (Boras et al., 2021; Owen et al., 2021).

Then, for each of the compounds, we started to grow the virus at the EC_{50}, doubling the drug amount every two passages to increase selective pressure while allowing the virus to replicate (Fig. 1b). In parallel, we performed virus passages in the absence of antiviral molecules to identify cell line adaptation mutations. We performed the experiment with 3 replicates of each condition. To assess the emergence of potential resistance mutations at passage 8, we sequenced the NSP5 gene -which contains the 3CLpro region- but found no mutations. As it was not possible to further increase the concentration of antiviral molecule in the supernatant, we carried out 8 additional passages at the maximum concentration (8 times higher than the EC_{50}). Throughout the experiment, we were able to maintain a stable level of viral replication without any remarkable drop in viral load (Fig. 1c).

By sequencing full viral genomes from all experimental conditions at passage 16, we identified mutations in the 3CLpro region, including some that were conserved across all replicates (Fig. 1d).

All three replicates of the cultures performed in the presence of nirmatrelvir exhibited the T21I mutation. The other mutations -T304I, L50F, E166A-were observed in one out of three replicates. We observed T21I either alone (replicate A3), combined with T304I (A2), or combined with both L50F and E166A (A1). All four mutations have been previously described as conferring nimatrelvir resistance (Hu et al.,

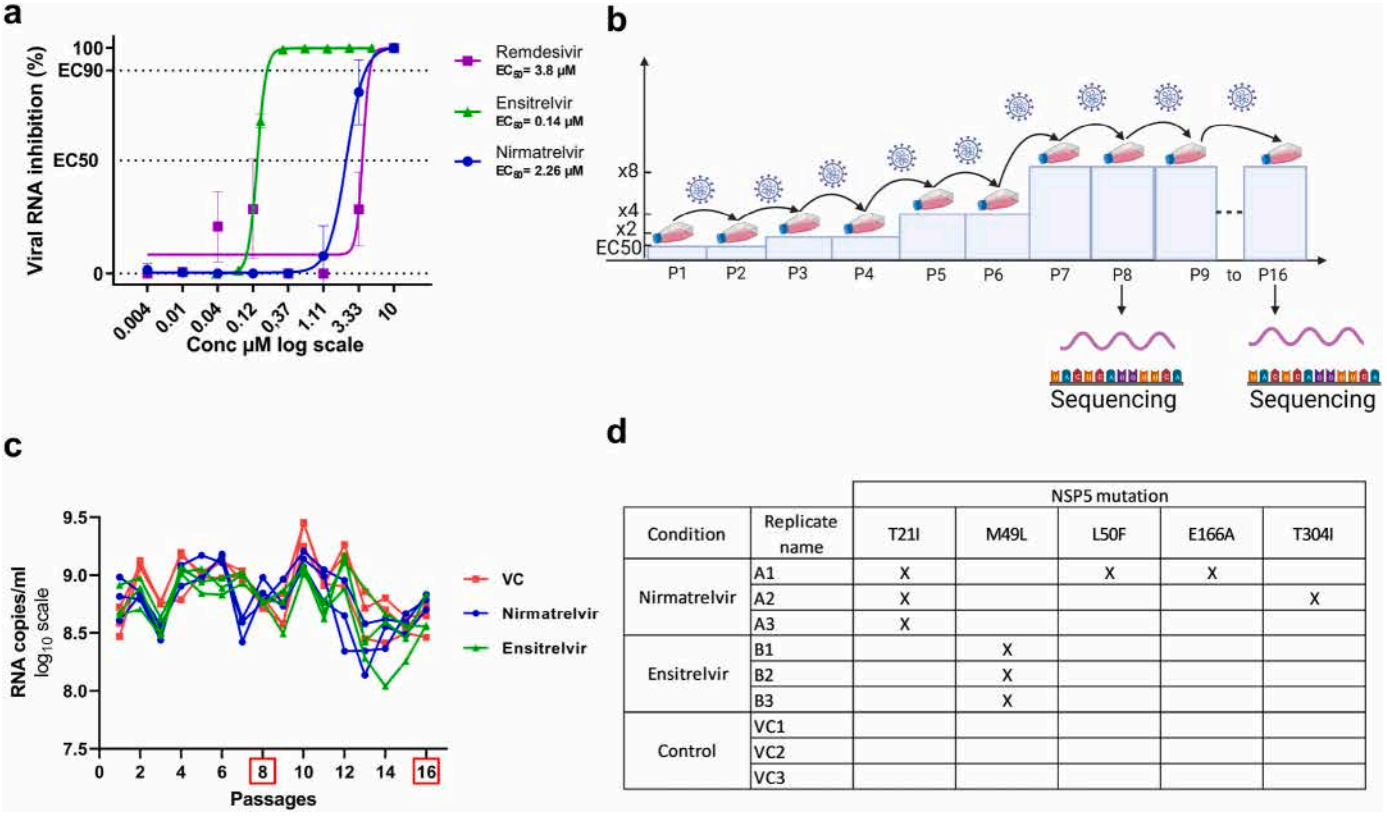

Condition	Replicate name	NSP5 mutation				
		T21I	M49L	L50F	E166A	T304I
Nirmatrelvir	A1	X		X	X	
	A2	X				X
	A3	X				
Ensitrelvir	B1		X			
	B2		X			
	B3		X			
Control	VC1					
	VC2					
	VC3					

Fig. 1. Generation of nirmatrelvir and ensitrelvir resistant strains. a) Pilot experiment to determine the EC_{50s} of nirmatrelvir and ensitrelvir. b) Graphical representation of the strategy used to obtain resistant strains. c) Viral replication measured by the amount of viral RNA at each passage in each replicate. d) Table of NSP5 amino acid mutations obtained at passage 16 in the different replicates.

2023; Iketani et al., 2023; Kawashima et al., 2023).

In the case of ensitrelvir, we only observed a single mutation, M49L, conserved across the three replicates. This mutation has already been described both in clinical isolates (Ip et al., 2023; Kawashima et al., 2023) and following experiments conducted *in vitro* (Kiso et al., 2023b) and shown to reduce sensitivity to the drug.

4.2. In vitro characterization of resistant strains

To characterize our mutant strains *in vitro*, we first monitored viral replication in VeroE6 TMPRSS2 cells in the absence of compound (Fig. 2a), using a low MOI (0.02), and a RT-qPCR assay.

Based on molecular viral load, we found no significant difference among the strains tested. These results are in line with the literature for T21I, T21I + T304I (Iketani et al., 2023) and M49L (Kiso et al., 2023b). They indicate that the mutations emerged in cell culture in the presence of nirmatrelvir and ensitrelvir do not alter significantly *in vitro* replication (Fig. 2a).

Using a dose-response approach, we then characterized the sensitivity of these strains to the two protease inhibitors, using remdesivir as a control. In addition to our wild-type reference strain (BavPat), we tested one of the strains that had undergone the same number of passages as the resistance mutants but without inhibitors (VC3). For the remdesivir control, we obtained very similar EC_{50} values for the 8 viruses tested, with a maximum variation of 0.5 μM in their EC_{50} (Fig. 2d–Table 1). This indicates that the 16 passages in culture did not alter the sensitivity of the strains to remdesivir or their basic replication properties.

In the ensitrelvir sensitivity analysis, the VC3 strain at 16 passages showed a sensitivity very close to that of the BavPat strain, with an EC_{50} of 0.49 μM versus 0.51 μM. This rules out an effect of the number of passages on sensitivity (Fig. 2b–Table 1). Strains selected in the presence of nirmatrelvir (nirmatrelvirR) showed a slightly reduced sensitivity to ensitrelvir (3 to 9-fold). On the other hand, the three M49L ensitrelvir-resistant (ensitrelvirR) mutants showed a great decrease in sensitivity (around 40-fold), indicating that this mutation does confer resistance to ensitrelvir (Fig. 2b–Table 1).

In the nirmatrelvir sensitivity analysis, the VC3 strain showed a

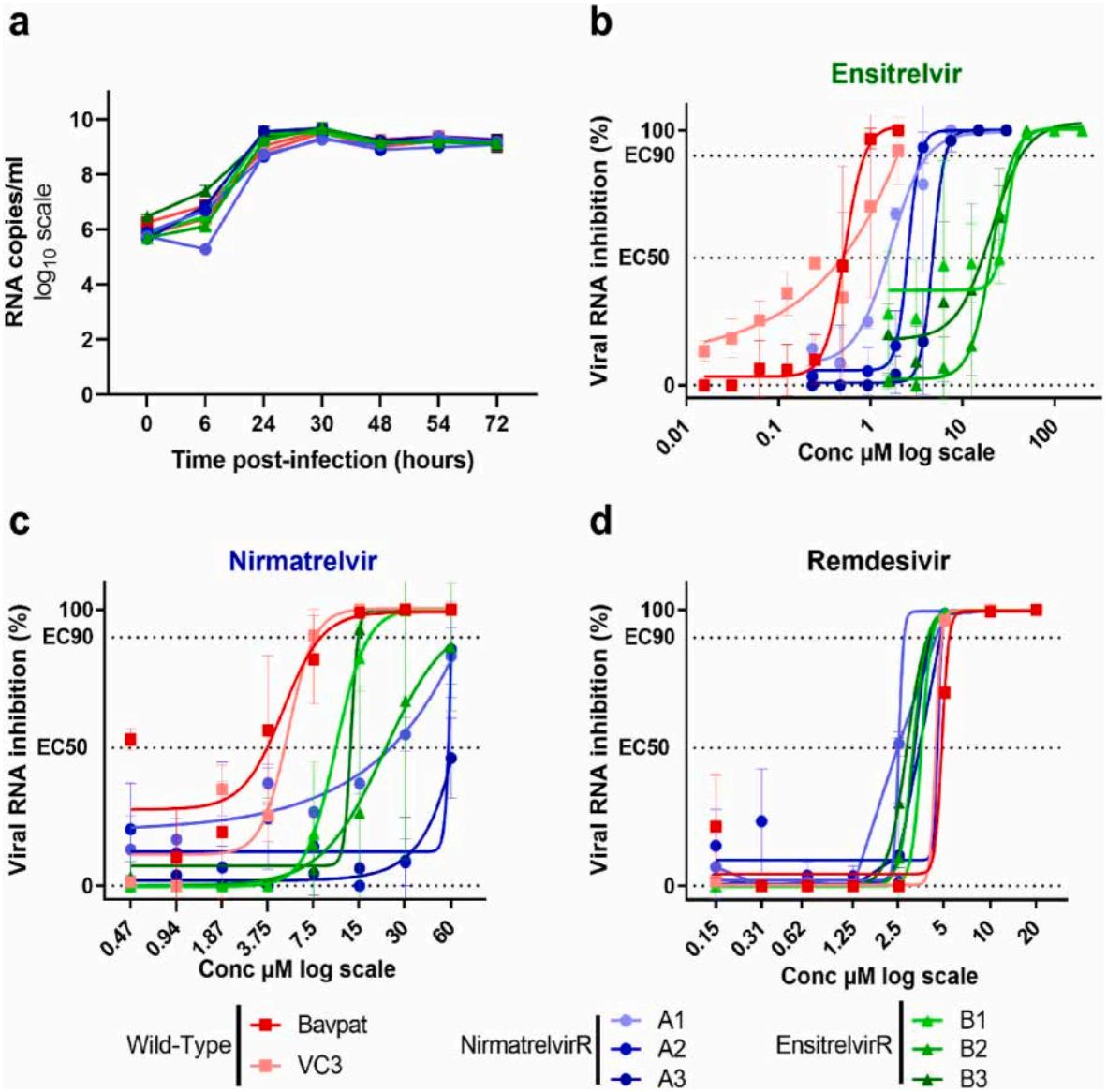

Fig. 2. In vitro characterization of nirmatrelvir and ensitrelvir resistant strains. a) Kinetics of replication in VeroE6 TMPRSS2 cells Data presented are from two technical replicates and error bars show mean ± s.d; Dose response curves reporting the susceptibility of SARS-CoV-2 mutants and two wild type strain against b) ensitrelvir c) nirmatrelvir and d) remdesivir. Data presented are from three technical replicates in VeroE6-TMPRSS2 cells, and error bars show mean ± s.d.

Table 1

Activity of ensitrelvir, nirmatrelvir and remdesivir against wild type and mutants strains. Interpolated EC_{50} values are expressed in μM. Fold change reductions were calculated in comparison with the EC_{50} of the BavPat strain. F.c: fold change.

		Wild type		ensitrelvirR			nirmatrelvirR		
		Bavpat	VC3	B1	B2	B3	A1	A2	A3
nirmatrelvir	EC_{50} (μM)	3.7	4.8	10.5	22.3	13.1	24.0	57.5	62.2
	EC_{90} (μM)	8.4	7.6	17.3	69.5	14.7	>60	>60	>60
	Fold change	-	1.3	2.8	6.0	3.5	6.5	15.5	16.8
ensitrelvir	EC_{50} (μM)	0.5	0.5	25.0	20.3	22.7	1.5	2.5	4.8
	EC_{90} (μM)	0.9	2.0	39.6	36.1	37.0	4.2	3.5	6.6
	Fold change	-	1.0	49.0	39.9	44.5	3.0	5.0	9.3
remdesivir	EC_{50} (μM)	4.8	4.4	3.5	3.1	2.8	2.5	4.5	3.2
	EC_{90} (μM)	5.4	4.8	4.1	3.9	3.9	2.7	4.8	4.0
	Fold change	-	0.9	0.7	0.7	0.6	0.5	0.9	0.7

f.c<5 | 5<f.c<10 | 10<f.c<100

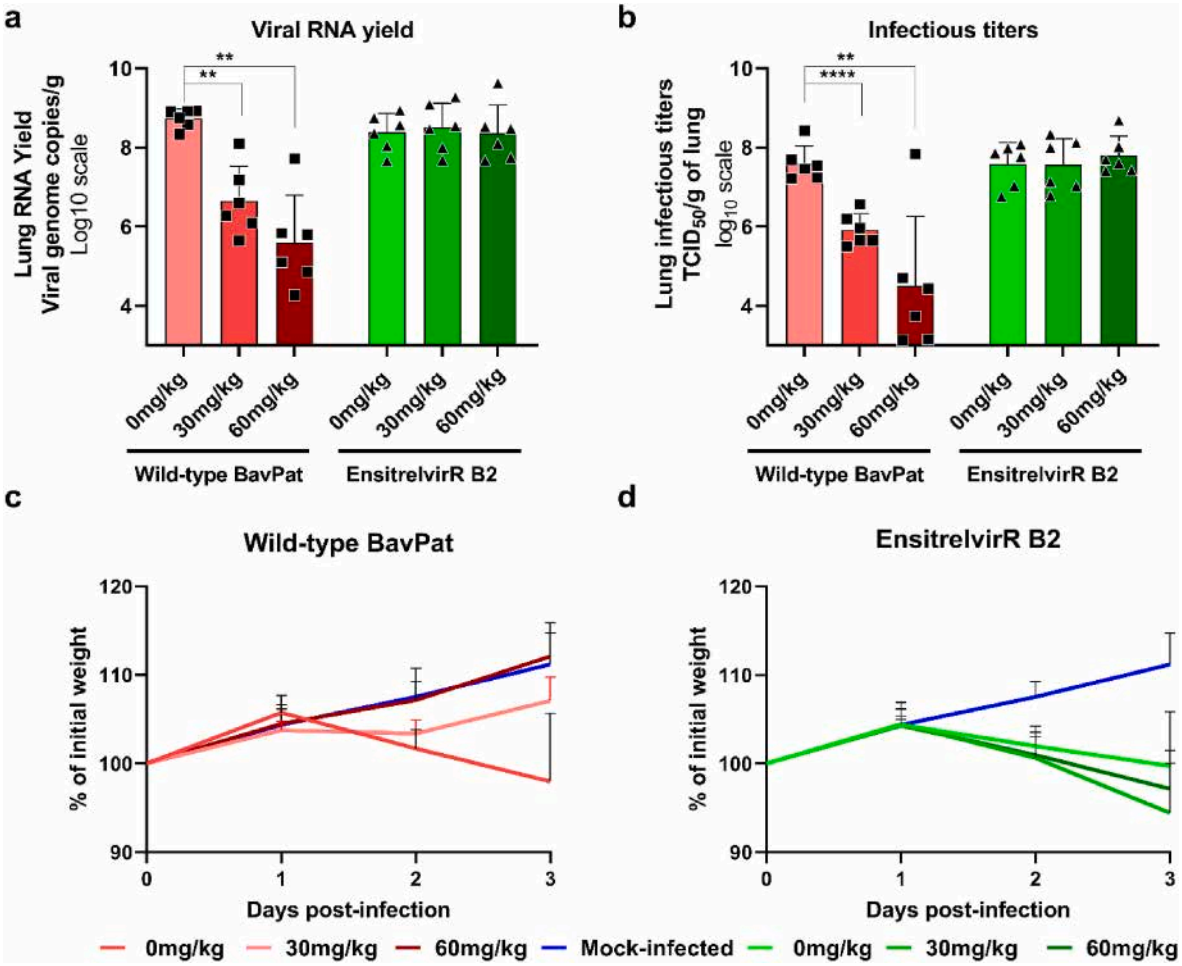

Fig. 3. Antiviral activity of oral ensitrelvir treatment in a hamster model against wild type and resistant SARS-CoV-2 strains

Groups of 6 hamsters were intranasally infected with 10^4 TCID50 of virus. Animals received ensitrelvir orally twice a day at 0 (untreated group), 30 or 60 mg/kg a) Viral replication in lung based on viral RNA yields at day 3 post infection (measured using an RT-qPCR assay) expressed in viral genome copies/g of lung. b) Viral replication in lung based on infectious titers at day 3 post-infection (measured using a TCID50 assay) expressed in TCID50/g of lung. c-d) Clinical course of the disease (n = 6 animals/group). Normalized weight at day n was calculated as follows: % of initial weight of the animal at day n. Data represent mean ± SD. Two-sided statistical analysis was performed using Shapiro-Wilk normality test and Student t-test, ** and **** indicate and average significant value lower than that of the untreated group, with a p-value ranging between 0.001 and 0.01 and lower to 0.0001 respectively.

sensitivity close to that of the BavPat strain, with an EC_{50} of 4.82 μM versus 3.70 μM (Fig. 2c Table 1). As before, two profiles were observed for the mutant strains (Fig. 2c Table 1): ensitrelvirR strains showed a slightly reduced sensitivity to nirmatrelvir (3 to 6-fold). On the other hand, the three nirmatrelvirR mutants showed a greater decreased in sensitivity (6–17-fold) (Fig. 2c Table 1). Interestingly, strains nirmatrelvirR-A2 and nirmatrelvirR-A3 showed the greatest resistance, despite having only one and two mutations, respectively. These results confirm that the T21I mutation and the combinations T21I-T304I and T21I-L50F-E166A do confer resistance to nirmatrelvir.

4.3. Ensitrelvir is not efficacious against M49L ensitrelvir -resistant strain in vivo

Nirmatrelvir mutants have already been extensively studied (Heilmann et al., 2022; Hu et al., 2023; Iketani et al., 2023; Kiso et al., 2023a) but the ensitrelvir resistance mutation M49L has never been evaluated alone *in vivo* in an antiviral susceptibility assay. To assess the ability of this mutation to confer resistance to ensitrelvir *in vivo*, we used a hamster model of SARS-CoV-2 infection previously developed for antiviral evaluation (Driouich et al., 2021, 2022; Touret et al., 2021b). We infected groups of 6 hamsters intranasally with either the wild type virus (BavPat), or M49L-R strain (B2). In addition to untreated groups, hamsters were administered 30 or 60 mg/kg of ensitrelvir orally twice a day. This regimen has previously been validated in two murine models (Kiso et al., 2023b; Unoh et al., 2022). It should be noted that in our study, unlike the one exploring loss of sensitivity to ensitrelvir *in vivo*, we used the strain from repeated passages and not generated by reverse genetics.

We observed that the M49L-ensitrlevirR strain and the wild type exhibited similar levels of replication in lungs of untreated hamster (no statistical differences) both in terms of viral RNA yield and infectious titers (Fig. 3 a and b). Regarding clinical follow-up, both the M49L-R strain and the wild-type induced a similar weight loss in hamsters (Fig. 3 c and d). These results show that, as observed *in vitro*, the selection process for resistance mutations has not deeply altered the replication characteristics and the pathogenicity of this strain in our model.

Regarding the antiviral effect of ensitrelvir on the wild-type strain, we observed a significant decrease in the amount of viral RNA and infectious titer in lungs, with a dose-response effect (Fig. 3 a and b). Furthermore, animals treated with 60 mg/kg had a similar clinical follow-up to uninfected hamsters with no statistical differences in weight change, suggesting a beneficial effect of treatment on clinical outcome (Fig. 3 c and Supplemental Fig. 1). Animals treated with 30 mg/kg had an intermediate clinical follow-up between untreated infected hamsters and uninfected hamsters, with a similar trend to uninfected hamsters despite a decline between day 1 and 2 (Fig. 3 c and Supplemental Fig. 1). These results indicate significant antiviral activity of ensitrelvir at both doses tested on the wild-type strain.

Regarding the antiviral effect of ensitrelvir on the resistant strain, we observed no significant decrease in viral RNA levels or infectious titers in lungs compared to control, regardless of the dosing regimen (Fig. 3 a and b). Furthermore, animals treated with 30 and 60 mg/kg had a clinical follow-up similar to untreated infected hamsters with no statistical differences in weight change to untreated infected hamsters, suggesting no beneficial effect of treatment on clinical outcome (Fig. 3d and Supplemental Fig. 1). These results indicate a lack of efficacy of ensitrelvir at both doses tested on the mutant strain containing the M49L mutation in NSP5. This result is in line with that obtained with the M49 L/E166A double mutant in the same hamster model (Kiso et al., 2023b), and demonstrates the ability of M49L to confer resistance to ensitrelvir even if in the absence of E166A.

4.4. The M49L mutation increased in prevalence over the last 6 months

The emergence of resistance mutations can drastically limit the use of the antiviral therapy affected. Resistance may emerge during prolonged use of the molecule in a patient with ongoing viral replication but can also occur naturally – without any specific selective pressure due to the use of the molecule in question. Our experiments show that the M49L mutation alone can confer resistance to ensitrelvir and previous reports have described M49L in circulating SARS-CoV-2 variants (Ip et al., 2023; Kawashima et al., 2023). The prevalence of this mutation in recent months and in particular, since the commercialization of ensitrelvir in Japan, has, however, not been reported.

We therefore searched on GISAID for all SARS-CoV-2 sequences carrying the M49L mutation. We found that, as of October 30, 2023, only 267 (0.00165 %) of the 16, 167, 749 SARS-CoV-2 sequences available on GISAID present an M to L amino acid substitution at position 49 in the NSP5 gene. Using sequence collection dates, we evaluated the distribution over time of all M49L-carrying SARS-CoV-2 sequences. We found that M49L was first reported on the August 13, 2020, and has been observed almost monthly since then (Fig. 4a), with an apparent global prevalence of 0.00168 % (total number of sequences with collection date on or after August 13, 2020: 15, 929, 475). When looking at the most recent time span, we found that more M49L-carrying sequences have been reported between May and October 2023 (count: 154; prevalence: 0.036 %) than over the previous 21 months (count: 113 M49L; prevalence: 0.0007 %). These numbers indicate that while M49L corresponds to a very small proportion of the sequences observed until today, its prevalence has increased during the last 6 months.

The repeated observations of low numbers of M49L-carrying sequences since the first year of the pandemic suggest that the mutation has emerged on multiple occasions and in several SARS-CoV-2 lineages. To determine the Pango lineage of each of the 267 sequences with the M49L mutation, we used the Pangolin online lineage assigner (O'Toole et al., 2021). We found that M49L-carrying sequences are distributed across 90 different lineages, including Alpha, Delta, and Omicron, with up to 31 sequences belonging to the same lineage (Fig. 4b–Supp. Table 1). The most prevalent lineages among M49L-carrying sequences are EG.5.1.1 (11.6 %), XBB.1.9.1 (5.6 %), and EG.5.1 (4.9 %). These three lineages are "active" (last observed less than a year ago) and classified either as "variant of interest" (VOI) or as "variant under monitoring" (VUM) by the WHO("Tracking SARS-CoV-2 variants and n. d"). Overall, these results indicate that NSP5 M49L can emerge in multiple genomic backgrounds and is present in active, currently prominent, lineages.

4.5. The recent increase in the prevalence of M49L appears to be linked to a specific selective pressure in Japan

Resistance against an antiviral therapy may occur naturally in circulating lineages but the use of a drug may favor the emergence of resistance mutations. Using the collection dates of M49L-carrying sequences, we showed that their proportion has been multiplied by more than 50 times in the last 6 months. Several scenarios may explain this increase in observation frequency: (i) a specific selective pressure; (ii) a more favorable genomic background; (iii) increased transmission.

The increased prevalence of the M49L resistance mutation observed in this study may be due to the existence of specific selective pressure, *i.e.* the use of the drug to which the compound confers resistance, ensitrelvir. The only country where this drug is used is Japan, where it first received an emergency use approval in November 2022, and was made commercially available in April 2023 ("Xocova to Be Commercially," n. d.). When we evaluated the spatial distribution -in terms of country of origin-of M49L sequences, we found that Japan is by far the most important country of origin for M49L sequences, with 59.9 % of sequences originating in Japan overall, a number that increases to 88.3 % when considering only collection dates between May and October 2023 (Figs. 4c and 5a). These results indicate that the vast majority of the M49L-carrying sequences collected over recent months originate from Japan.

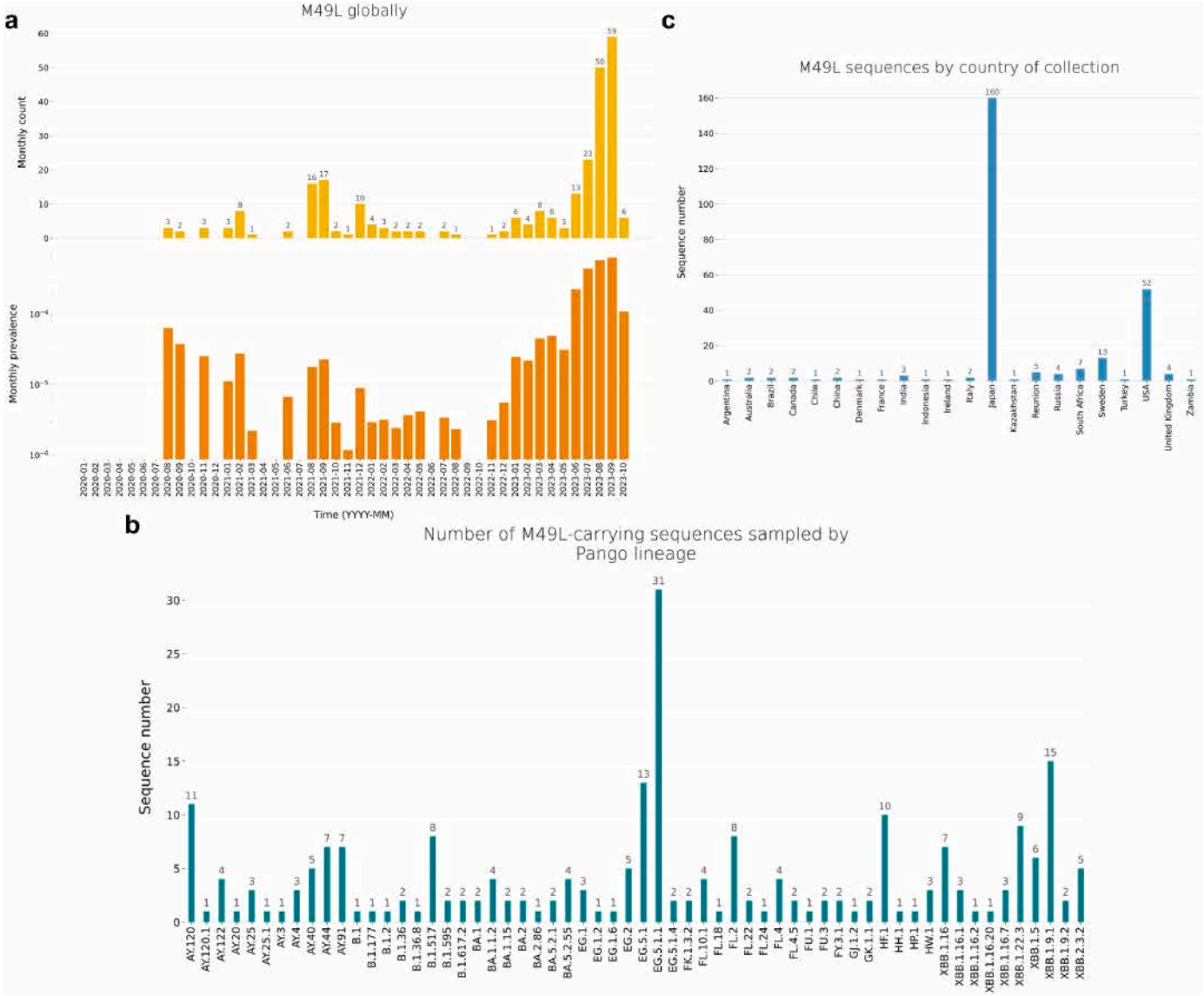

Fig. 4. M49L distribution in time, space, and across lineages. a) Global monthly counts (upper panel) and prevalences (lower panel) of M49L-sequences, based on all SARS-CoV-2 genomes publicly available on GISAID as of 2023–11-13. b) Number of M49L sequences observed by lineage, for each of the 60 Pango lineages observed most frequently among M49L sequences. c) Number of M49L sequences observed by country of collection.

When analyzing the time distribution of all M49L-sequences from Japan, we found that M49L has been observed only 4 times before December 2022 but almost monthly since then (Fig. 5b), with especially high monthly prevalence values (above 0.2 %) since June 2013. The timing of the increase in the prevalence of M49L and the origin of M49L sequences both align well with the use of Xocova® in Japan, suggesting that this selective pressure may favor the emergence of the mutation.

Another factor that may however, explain the recent increase in M49L sequences overall and in Japan more specifically, is the local circulation of lineages with a genomic background more favorable for the emergence of the mutation. To evaluate if recent M49L-sequences were associated with a specific genomic background, we analyzed their lineage distribution. We found that between May and October 2023, M49L occurred in 44 different lineages globally and in 40 different lineages in Japan including, EG.*, FL.*, GJ.*, HF.*, XBB.1.9.*, and XBB.1.16.* lineages (Fig. 5c). These results indicate that multiple distinct lineages can accommodate the M49L mutation.

When considering M49L-sequences from the most prevalent lineage, EG.5.1.1, 93.5 % of them appear to originate in Japan, and only 3.2 % both in the US and in Canada. Based on GISAID data, EG.5.1.1 appears to have circulated to levels on the same order of magnitude (or greater) to that observed over the last 6 months in Japan (7.6 % of 37,550 total sequences), in the US (3.8 % of 146,709 total sequences), in Canada (6.8 % of 46,555 total sequences), and in China (18.2 % of 34,404 total sequences). If the increase in M49L prevalence was driven by the genomic background of EG.5.1.1 being more favorable, this mutation would have also emerged more frequently in other locations where the lineage has established sustained transmission. These observations indicate that the recent increase in M49L prevalence is not driven by a single -or a few- more favorable genomic background.

4.6. Repeated emergence, rather than increased transmission, contributed to the recent increase in M49L prevalence

Another phenomenon that may have participated in increasing the prevalence of M49L in recent month is the formation of large transmission chains by naturally-occurring M49L mutant. The distribution of recent M49L sequences across 44 different lineages suggests that increased emergence events, rather than increased transmission, fueled the rise in M49L detections. However, the presence of a large

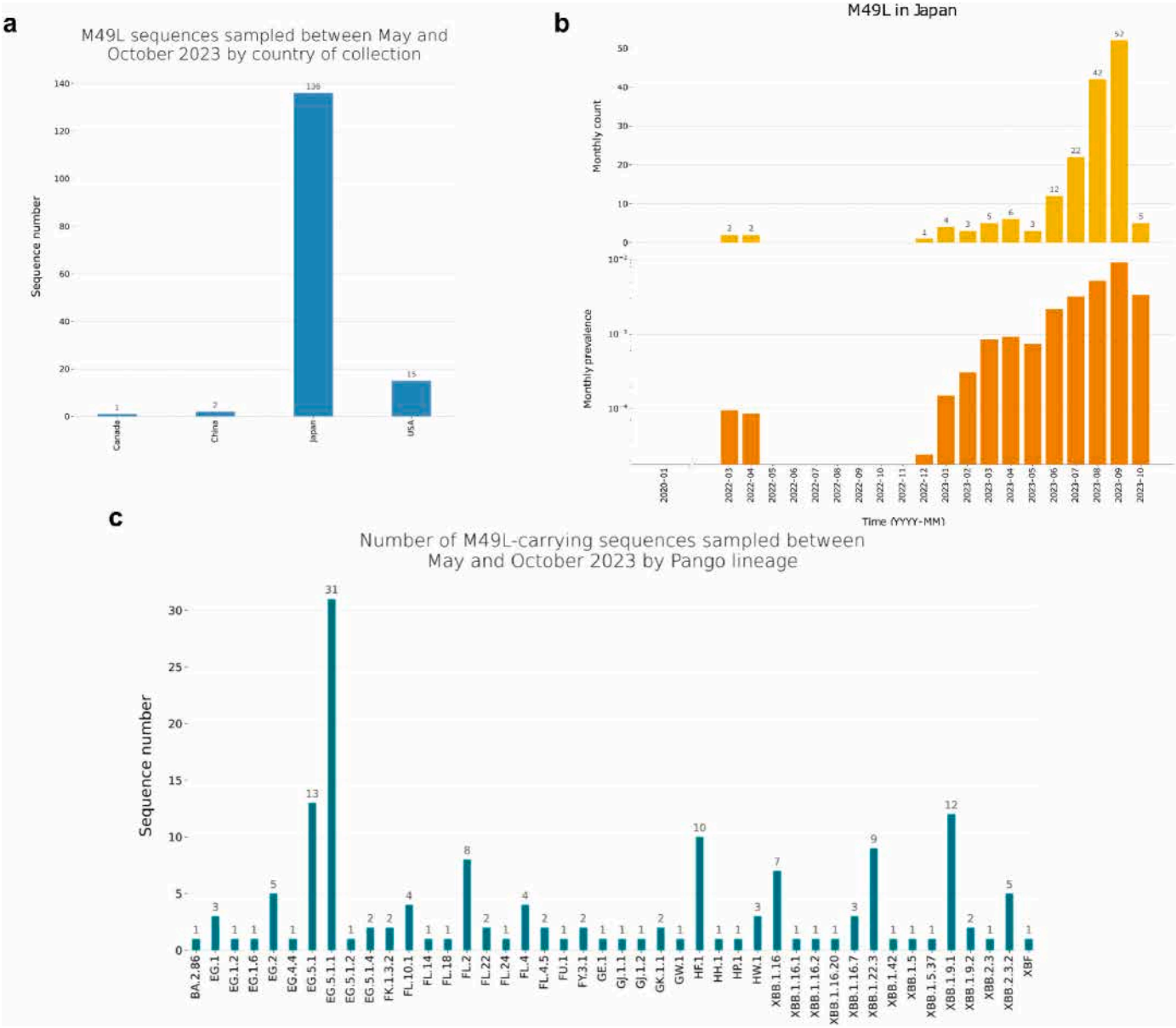

Fig. 5. M49L distribution in time, space and, across lineages between May and October 2023 in Japan. a) Number of M49L sequences observed by country of collection for sequences collected between May and October 2023. b) Monthly counts (upper panel) and prevalences (lower panel) of M49L-sequences in Japan, based on all SARS-CoV-2 genomes publicly available on GISAID as of 2023–11-13. c) Number of recent M49L sequences (collection date between October and May 2023) observed by lineage, for each of the Pango lineages observed among recent M49L sequences.

transmission chain within the main lineage EG.5.1.1 may have been an exacerbating factor.

To determine whether recent M49L-carrying sequences from the most prominent lineage, EG.5.1.1, correspond to a single or multiple emergence events, we performed a phylogenetic inference based on a set of publicly available SARS-CoV-2 genomes. Using a maximum-likelihood approach, we inferred the phylogenetic relationships between all M49L-carrying EG.5.1.1 sequences and a set of EG.5.1.1 sequences collected between July and October in Japan and North America (to match the spatio-temporal distribution of the M49L genomes). In the resulting phylogeny, we identified 12 different M49L emergence events, associated either with single tips, or with entire well-supported clades encompassing up to 10 sequences (Fig. 6). Our findings were broadly similar across 10 inference replicates. These results show that recent M49L-carrying sequences do not form a single clade – the mutation emerged at least on 12 independent occasions within that lineage.

5. Discussion

In this study, we experimentally generated six viruses carrying resistance mutations to clinical stage SARS-CoV-2 protease inhibitors. We obtained three viruses with different sets of mutations for nirmatrelvir. For ensitrelvir, on the other hand, all three strains had the same mutation M49L. *In vitro* characterization showed that nirmatrelvir-resistant strains had low resistance to ensitrelvir, but higher resistance to nirmatrelvir. Similarly, ensitrelvir-resistant strains showed low resistance to nirmatrelvir but much higher resistance to ensitrelvir. Finally, we investigated *in vivo* the resistance of an EnsitrelvirR M49L strain to two regimens of ensitrelvir and found that it completely escaped the inhibition induced by this antiviral compound.

We obtained resistance mutations after 16 passages with an increasing concentration of nirmatrelvir, which is similar to what has already been shown by Iketani and colleagues (Iketani et al., 2023). Indeed, these specific mutations have already been obtained using a

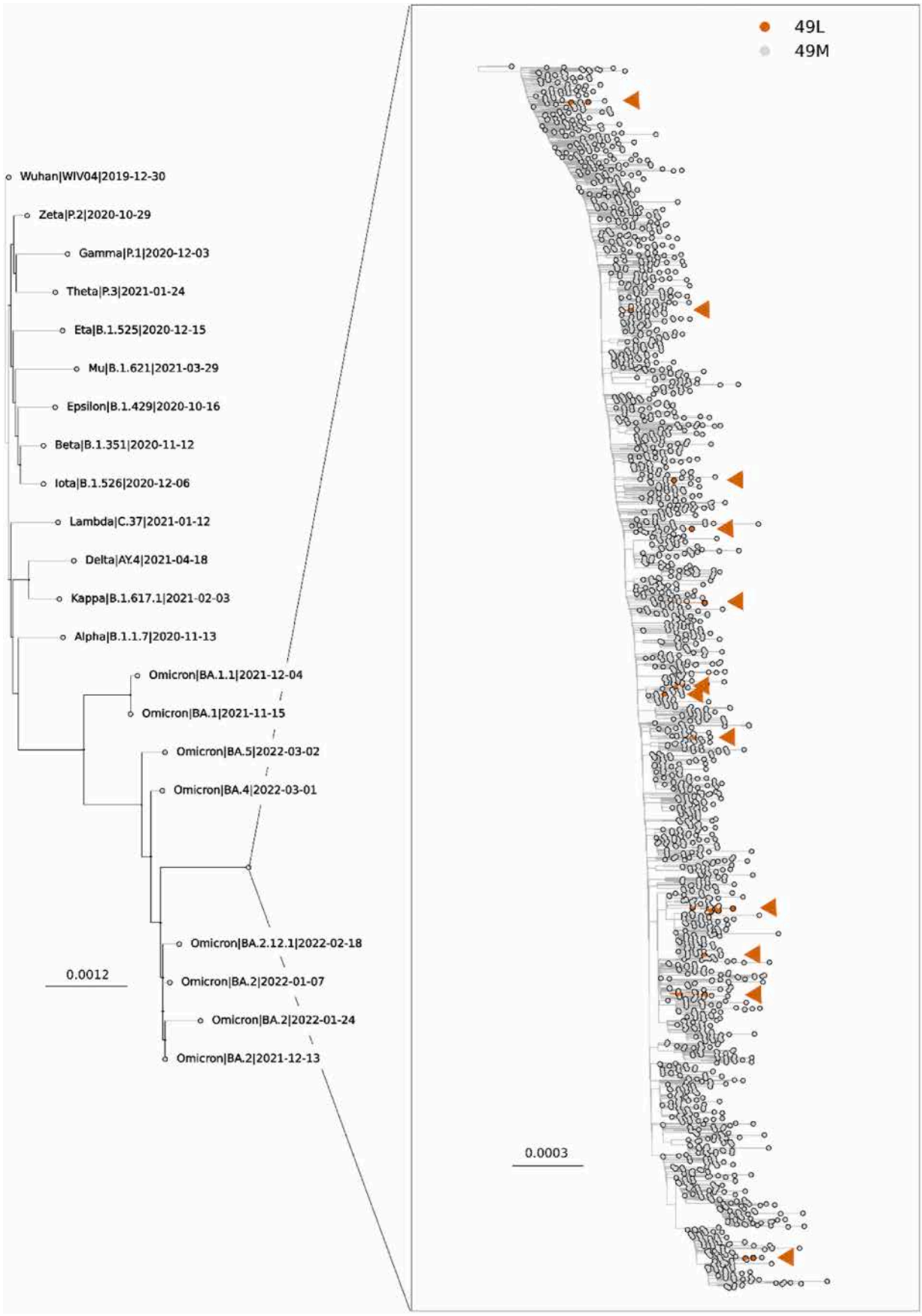

Fig. 6. Maximum-likelihood phylogeny with a zoom on the EG.5.1.1 lineage. Branches and tips associated with M49L-carrying sequences are highlighted in orange. Orange arrows indicate M49L emergence events.

similar approach: the T21I mutation was generated alone or in combination with E166V or T304I, exactly as in our study. This mutation, along with T304I, was predominantly acquired as initial mutation (Iketani et al., 2023). Interestingly, in the VeroE6 TMPRSS2 cell line, we obtained a mutation at residue 166, whereas in the study by Iketani and colleagues (Iketani et al., 2023) a mutation at this position only appeared in HUH.7 and not in VeroE6, and the authors supposed that it was specific to this cell line. The mutation on residue 166 had already been described and was shown to reduce viral replicative fitness, but this fitness could be restored by the addition of the T21I mutation (Iketani et al., 2023). In our study, we confirmed this observation by showing that the replication capacity of our mutant (A1) carrying both T21I and E166A was the same as that of the wild type. Finally the mutation at residue 166 was the only one obtained in the substrate binding site; the others are situated at a distal position from nirmatrelvir predicted binding site (over 5 Å(Iketani et al., 2023)).

For ensitrelvir, we obtained three viruses with the same mutation, M49L. This mutation has already been obtained in a similar experiment, but with a shorter passage number (Kiso et al., 2023a). It is also present in circulating isolates of SARS-CoV-2 (Hu et al., 2023; Kawashima et al., 2023; Moghadasi et al., 2023b; Noske et al., 2023).

In a report identifying M49I as an ensitrelvir resistance mutation its visualization in complex with the 3CLpro shows that the greater hydrophobicity of isoleucine, compared to the methionine, caused the inhibitor to move to another site, which affects its antiviral activity (Noske et al., 2023). According to another study, the presence of a leucine instead of an isoleucine at this position could cause a greater resistance due the gamma-carbon branching of the leucine side chain, which is nearer to H41 one of the catalytic dyad in its active site (Moghadasi et al., 2023b; Unoh et al., 2022).

We found *in vitro* moderate cross resistance between NirmatrelvirR strains and ensitrelvir, and the same for EnsitrelvirR strains and nirmatrelvir, in accordance with previous studies (Iketani et al., 2023; Moghadasi et al., 2023b). This suggests that replacing one of the two compounds with the other could compensate for the emergence of a resistance mutation during treatment.

We observed the greatest loss in activity with the couple ensitrelvir/M49L with a ~40-fold reduction in susceptibility for our three ensitrelvirR strains. This mutation had already been tested, alone, in two distinct enzymatic assays (Moghadasi et al., 2023a, 2023b) and in a VSV based cleavage system (Moghadasi et al., 2023b), with observed fold change values of 21.4, 25.4 and 10 respectively. In the only previous study that explored the effect of this mutation with a replicative virus (a mutated Delta strain generated by reverse genetic (Kiso et al., 2023b)) M49L was associated with a 37.4 fold change in a focus reduction assay (Kiso et al., 2023a). This result is perfectly in line with our observation with the same range of reduction despite the use of the strain generated from repeated passages in a different variant backbone. The fact that we found the same effect for a single amino acid mutation but with a different backbone not only confirms but reinforces our result.

In the abovementioned study, the authors only studied the *in vivo* antiviral resistance of the M49 L/166 A mutation pair (Kiso et al., 2023b). Regarding the single mutation M49L, they only explored its impact on the *in vitro* replication fitness and the *in vivo* pathogenicity. We went a step further and explored the effect of this single mutation on ensitrelvir sensitivity, using both the ensitrelvir dose referred to in the study above (60 mg/kg twice daily) (Kiso et al., 2023b) and a lower dose as in the original S-217622/ensitrelvir article (30 mg/kg twice daily) (Unoh et al., 2022). When animals were infected with the ensitrelvirR strain, we observed no antiviral activity for either of ensitrelvir dose regimen and, in contrast to what was observed with the wild-type strain, no clinical improvement. This implies that the M49L mutation can be solely responsible for *in vivo* resistance. The same result at the highest regimen was observed *in vivo* with the double mutants M49 L/E166A (Kiso et al., 2023b). The *in vitro* fold change of this combination is almost 200 (Kiso et al., 2023b). Our result implies that a single mutation inducing a change in susceptibility of 40, *i.e.* five times lower, is enough to make ensitrelvir treatment ineffective in our animal model.

In the current study, we detailed a recent increase in the prevalence of M49L-carrying sequences, linked it to a specific region, Japan, and showed that this increase is concomitant with the use of ensitrelvir in the country (emergency approval and then commercialization) rather than with the emergence of a more favorable viral genomic background. These initial results are concerning and warrant further investigation, especially as several countries are currently considering the drug for emergency approval ("Drugmaker Shionogi inks deal to market COVID pill in China," n. d.; "Xocova Filed for Conditional Approval in South Korea" n. d.). It is crucial to better characterize the conditions and frequency of emergence of the M49L mutation in patients treated with ensitrelvir. If an increased risk of resistance emergence during patient treatment is confirmed, genomic monitoring may allow to both optimize the medical efficacy of the treatment provided and prevent the spread of resistant strains. In case of resistance, it would still be possible to replace ensitrelvir with nirmatrelvir, given the low level of cross-resistance between the two molecules. However, this would be difficult for patients who had received ensitrelvir treatment in the first instance, due to a contraindication to ritonavir, which is present in Paxlovid®, the pharmaceutical formulation of nirmatrelvir.

To evaluate the potential duration of transmission for EG.5.1.1 M49L-mutants, we calculated minimum clade-durations for all M49L-clades by calculating the difference in time between the earliest and latest sampling dates among sequences of a given clade. We found that clade-duration could be up to 58 days for M49L clades belonging to the EG.5.1.1 lineage. This first assessment however, is based on a small number of clades (3) and on a limited sampling of the recent circulating diversity of SARS-CoV-2. For computational tractability reasons we focused our phylogenetic analysis on sequences from a single lineage (EG.5.1.1), specific countries (Japan, North America), and subsampled our dataset. We believe that it is of the utmost importance to pursue these investigations and to continue to monitor the ability of M49L-carrying lineages to establish sustained transmission and to assess the risk of fixation of the mutation.

Finally, while we showed that the use of ensitrelvir is probably a driver of the increased frequency of emergence of M49L in recent months in Japan, it is likely that the 107 early sequences carrying M49L (identified between August 2020 and October 2023) emerged spontaneously as the antiviral was not in use before November 2022. The natural occurrence of strains carrying M49L may thus facilitate the emergence of resistance to ensitrelvir.

Other variations in the NSP5 protein provide resistance to ensitrelvir and have been observed in circulating isolates. They may present a risk of increased emergence in case of wide use of ensitrelvir, akin to what was showed for M49L in the present study. In particular, the mutation M49I provides resistance *in vitro* (Moghadasi et al., 2023b) and is present in 2188 SARS-CoV-2 sequences on GISAID (as of October 30th). For this mutation however, we found no apparent increase in prevalence over recent months in Japan (Supplemental Fig. 2a) with most M49I sequences observed between June and December 2021. Along with the fact that M49I has never been observed in experiments of generation of ensitrelvir-resistant mutants (current study and in (Kiso et al., 2023b), this finding suggests that under selective pressure, the M49L mutation is preferred, likely because it provides greater resistance by generating a branching pattern more favorable to the disruption of a base stacking interaction with the inhibitor (Moghadasi et al., 2023b; Noske et al., 2023). In addition, the lower prevalence of M49I over recent months in Japan compared to M49L (Supplemental Fig. 2b) may be due to less favorable circulating genetic backgrounds, as most M49I sequences are associated with lineages AY.4 (714/2188 sequences) and AY.44 (172/2188), and circulated during the pre-Omicron period (Supplemental Figs. 2a and 2c). These results suggest the risk of emergence of resistance associated with M49I is currently lower than for M49L, but other mutations, in the 45–49 and other regions of M^{pro}, require

continuous monitoring in countries where ensitrelvir is, or will soon be, approved for use.

These findings argues in favor of genetic monitoring of circulating strains to ensure that the treatments administered retain their full effectiveness. In addition, the range of antiviral treatments available against SARS-CoV-2 has become worryingly limited, with most commercial monoclonal drugs losing their activity against the most recent variants. Obviously, there is still a need to develop other antivirals targeting other viral proteins to broaden the therapeutic armory, and possibly to develop dual therapies as has been done for other viral diseases.

CRediT authorship contribution statement

Hawa Sophia Bouzidi: Writing – review & editing, Writing – original draft, Visualization, Investigation, Formal analysis. **Jean-Sélim Driouich:** Writing – review & editing, Writing – original draft, Visualization, Methodology, Investigation, Formal analysis. **Raphaëlle Klitting:** Writing – review & editing, Visualization, Investigation, Formal analysis. **Ornéllie Bernadin:** Writing – review & editing, Visualization, Investigation, Formal analysis. **Géraldine Piorkowski:** Writing – review & editing, Investigation, Formal analysis. **Rayane Amaral:** Writing – review & editing, Investigation. **Laurent Fraisse:** Writing – review & editing, Funding acquisition. **Charles E. Mowbray:** Writing – review & editing, Funding acquisition. **Ivan Scandale:** Writing – review & editing, Conceptualization. **Fanny Escudié:** Writing – review & editing, Conceptualization. **Eric Chatelain:** Writing – review & editing, Funding acquisition, Conceptualization. **Xavier de Lamballerie:** Writing – review & editing, Resources, Funding acquisition. **Antoine Nougairède:** Writing – review & editing, Writing – original draft, Visualization, Resources, Methodology, Conceptualization. **Franck Touret:** Writing – review & editing, Writing – original draft, Visualization, Resources, Methodology, Investigation, Funding acquisition, Formal analysis, Conceptualization.

Declaration of competing interest

The authors declare that they have no known competing financial interests or personal relationships that could have appeared to influence the work reported in this paper.

Data availability

Data will be made available on request.

Acknowledgments

We thank Magali Gilles (UVE; Marseille), Gregory Moureau (UVE; Marseille) and Camille Placidi (UVE; Marseille) for their valuable technical contribution. We thank Edyth Parker for her recommendations on SARS-CoV-2 phylogenetic inference. We thank Pr. Drosten for providing the SARSCoV-2 strain through the European Research infrastructure EVA GLOBAL.

This work was supported by the European Virus Archive Global (EVA GLOBAL) funded by the European Union's Horizon 2020 research and innovation program under grant agreement No. 871029 and by DNDi under support by the Wellcome Trust Grant ref: 222489/Z/21/Z through the COVID-19 Therapeutics Accelerator. This work was supported by the ARBOGEN project, funded by the MSDAVENIR foundation. Part of the work was done on the Aix Marseille University antivirals platform "MaSC".

Appendix A. Supplementary data

Supplementary data to this article can be found online at https://doi.org/10.1016/j.antiviral.2024.105814.

References

Beigel, J.H., Tomashek, K.M., Dodd, L.E., Mehta, A.K., Zingman, B.S., Kalil, A.C., Hohmann, E., Chu, H.Y., Luetkemeyer, A., Kline, S., Lopez de Castilla, D., Finberg, R. W., Dierberg, K., Tapson, V., Hsieh, L., Patterson, T.F., Paredes, R., Sweeney, D.A., Short, W.R., Touloumi, G., Lye, D.C., Ohmagari, N., Oh, M., Ruiz-Palacios, G.M., Benfield, T., Fätkenheuer, G., Kortepeter, M.G., Atmar, R.L., Creech, C.B., Lundgren, J., Babiker, A.G., Pett, S., Neaton, J.D., Burgess, T.H., Bonnett, T., Green, M., Makowski, M., Osinusi, A., Nayak, S., Lane, H.C., 2020. Remdesivir for the treatment of Covid-19 — final report. N. Engl. J. Med. 383, 1813–1826. https://doi.org/10.1056/NEJMoa2007764.

Bloom, J.D., Gong, L.I., Baltimore, D., 2010. Permissive secondary mutations enable the Evolution of Influenza Oseltamivir resistance. Science 328, 1272–1275. https://doi.org/10.1126/science.1187816.

Boras, B., Jones, R.M., Anson, B.J., Arenson, D., Aschenbrenner, L., Bakowski, M.A., Beutler, N., Binder, J., Chen, E., Eng, H., Hammond, H., Hammond, J., Haupt, R.E., Hoffman, R., Kadar, E.P., Kania, R., Kimoto, E., Kirkpatrick, M.G., Lanyon, L., Lendy, E.K., Lillis, J.R., Logue, J., Luthra, S.A., Ma, C., Mason, S.W., McGrath, M.E., Noell, S., Obach, R.S., O' Brien, M.N., O'Connor, R., Ogilvie, K., Owen, D., Pettersson, M., Reese, M.R., Rogers, T.F., Rosales, R., Rossulek, M.I., Sathish, J.G., Shirai, N., Steppan, C., Ticehurst, M., Updyke, L.W., Weston, S., Zhu, Y., White, K.M., García-Sastre, A., Wang, J., Chatterjee, A.K., Mesecar, A.D., Frieman, M.B., Anderson, A.S., Allerton, C., 2021. Preclinical characterization of an intravenous coronavirus 3CL protease inhibitor for the potential treatment of COVID19. Nat. Commun. 12 (6055) https://doi.org/10.1038/s41467-021-26239-2.

Driouich, J.-S., Cochin, M., Lingas, G., Moureau, G., Touret, F., Petit, P.-R., Piorkowski, G., Barthélémy, K., Laprie, C., Coutard, B., Guedj, J., de Lamballerie, X., Solas, C., Nougairède, A., 2021. Favipiravir antiviral efficacy against SARS-CoV-2 in a hamster model. Nat. Commun. 12 (1735) https://doi.org/10.1038/s41467-021-21992-w.

Driouich, J.-S., Cochin, M., Touret, F., Petit, P.-R., Gilles, M., Moureau, G., Barthélémy, K., Laprie, C., Wattanakul, T., Chotsiri, P., Hoglund, R.M., Tarning, J., Fraisse, L., Sjö, P., Mowbray, C.E., Escudié, F., Scandale, I., Chatelain, E., de Lamballerie, X., Solas, C., Nougairède, A., 2022. Pre-clinical evaluation of antiviral activity of nitazoxanide against SARS-CoV-2. EBioMedicine 82 (104148). https://doi.org/10.1016/j.ebiom.2022.104148.

Drugmaker Shionogi inks deal to market COVID pill in China [WWW Document]. Nikkei Asia. n.d. https://asia.nikkei.com/Business/Pharmaceuticals/Drugmaker-Shionogi-inks-deal-to-market-COVID-pill-in-China, 11.14.23.

Hammond, J., Leister-Tebbe, H., Gardner, A., Abreu, P., Bao, W., Wisemandle, W., Baniecki, M., Hendrick, V.M., Damle, B., Simón-Campos, A., Pypstra, R., Rusnak, J. M., 2022. Oral nirmatrelvir for high-risk, nonhospitalized adults with covid-19. N. Engl. J. Med. 386, 1397–1408. https://doi.org/10.1056/NEJMoa2118542.

Heilmann, E., Costacurta, F., Moghadasi, S.A., Ye, C., Pavan, M., Bassani, D., Volland, A., Ascher, C., Weiss, A.K.H., Bante, D., Harris, R.S., Moro, S., Rupp, B., Martinez-Sobrido, L., von Laer, D., 2022. SARS-CoV-2 3CLpro mutations selected in a VSV-based system confer resistance to nirmatrelvir, ensitrelvir, and GC376. Sci. Transl. Med. 15, eabq7360. https://doi.org/10.1126/scitranslmed.abq7360.

Hoertel, N., Boulware, D.R., Sánchez-Rico, M., Burgun, A., Limosin, F., 2022. Prevalence of contraindications to nirmatrelvir-ritonavir among hospitalized patients with COVID-19 at risk for progression to severe disease. JAMA Netw. Open 5, e2242140. https://doi.org/10.1001/jamanetworkopen.2022.42140.

Hu, Y., Lewandowski, E.M., Tan, H., Zhang, Xiaoming, Morgan, R.T., Zhang, Xiujun, Jacobs, L.M.C., Butler, S.G., Gongora, M.V., Choy, J., Deng, X., Chen, Y., Wang, J., 2023. Naturally occurring mutations of SARS-CoV-2 main protease confer drug resistance to nirmatrelvir. ACS Cent. Sci. 9, 1658–1669. https://doi.org/10.1021/acscentsci.3c00538.

Hunter, J.D., 2007. Matplotlib: a 2D graphics environment. Comput. Sci. Eng. 9, 90–95. https://doi.org/10.1109/MCSE.2007.55.

Iketani, S., Mohri, H., Culbertson, B., Hong, S.J., Duan, Y., Luck, M.I., Annavajhala, M.K., Guo, Y., Sheng, Z., Uhlemann, A.-C., Goff, S.P., Sabo, Y., Yang, H., Chavez, A., Ho, D. D., 2023. Multiple pathways for SARS-CoV-2 resistance to nirmatrelvir. Nature 613, 558–564. https://doi.org/10.1038/s41586-022-05514-2.

Imai, M., Ito, M., Kiso, M., Yamayoshi, S., Uraki, R., Fukushi, S., Watanabe, S., Suzuki, T., Maeda, K., Sakai-Tagawa, Y., Iwatsuki-Horimoto, K., Halfmann, P.J., Kawaoka, Y., 2022. Efficacy of antiviral agents against omicron subvariants BQ.1.1 and XBB. New England J. Med. 0, null. https://doi.org/10.1056/NEJMc2214302.

Ip, J.D., Wing-Ho Chu, A., Chan, W.-M., Cheuk-Ying Leung, R., Umer Abdullah, S.M., Sun, Y., To, K.K.-W., 2023. Global prevalence of SARS-CoV-2 3CL protease mutations associated with nirmatrelvir or ensitrelvir resistance. EBioMedicine 91 (104559). https://doi.org/10.1016/j.ebiom.2023.104559.

Issues with SARS-CoV-2 sequencing data - SARS-CoV-2 coronavirus/nCoV-2019 Genomic Epidemiology [WWW Document], 2020. Virological. https://virological.org/t/issues-with-sars-cov-2-sequencing-data/473/1, 11.14.23.

Jin, Z., Du, X., Xu, Y., Deng, Y., Liu, M., Zhao, Y., Zhang, B., Li, X., Zhang, L., Peng, C., Duan, Y., Yu, J., Wang, L., Yang, K., Liu, F., Jiang, R., Yang, Xinglou, You, T., Liu, Xiaoce, Yang, Xiuna, Bai, F., Liu, H., Liu, Xiang, Guddat, L.W., Xu, W., Xiao, G., Qin, C., Shi, Z., Jiang, H., Rao, Z., Yang, H., 2020. Structure of Mpro from SARS-CoV-2 and discovery of its inhibitors. Nature 582, 289–293. https://doi.org/10.1038/s41586-020-2223-y.

Katoh, K., Standley, D.M., 2013. MAFFT multiple sequence alignment software version 7: improvements in performance and usability. Mol. Biol. Evol. 30, 772–780. https://doi.org/10.1093/molbev/mst010.

Kawashima, S., Matsui, Y., Adachi, T., Morikawa, Y., Inoue, K., Takebayashi, S., Nobori, H., Rokushima, M., Tachibana, Y., Kato, T., 2023. Ensitrelvir is effective

against SARS-CoV-2 3CL protease mutants circulating globally. Biochem. Biophys. Res. Commun. 645, 132–136. https://doi.org/10.1016/j.bbrc.2023.01.040.
Kiso, M., Furusawa, Y., Uraki, R., Imai, M., Yamayoshi, S., Kawaoka, Y., 2023a. In vitro and in vivo characterization of SARS-CoV-2 strains resistant to nirmatrelvir. Nat. Commun. 14 (3952) https://doi.org/10.1038/s41467-023-39704-x.
Kiso, M., Yamayoshi, S., Iida, S., Furusawa, Y., Hirata, Y., Uraki, R., Imai, M., Suzuki, T., Kawaoka, Y., 2023b. In vitro and in vivo characterization of SARS-CoV-2 resistance to ensitrelvir. Nat. Commun. 14 (4231) https://doi.org/10.1038/s41467-023-40018-1.
Korber, B., Fischer, W.M., Gnanakaran, S., Yoon, H., Theiler, J., Abfalterer, W., Hengartner, N., Giorgi, E.E., Bhattacharya, T., Foley, B., Hastie, K.M., Parker, M.D., Partridge, D.G., Evans, C.M., Freeman, T.M., de Silva, T.I., Angyal, A., Brown, R.L., Carrilero, L., Green, L.R., Groves, D.C., Johnson, K.J., Keeley, A.J., Lindsey, B.B., Parsons, P.J., Raza, M., Rowland-Jones, S., Smith, N., Tucker, R.M., Wang, D., Wyles, M.D., McDanal, C., Perez, L.G., Tang, H., Moon-Walker, A., Whelan, S.P., LaBranche, C.C., Saphire, E.O., Montefiori, D.C., 2020. Tracking changes in SARS-CoV-2 spike: evidence that D614G increases infectivity of the COVID-19 virus. Cell 182, 812–827. https://doi.org/10.1016/j.cell.2020.06.043 e19.
Minh, B.Q., Nguyen, M.A.T., von Haeseler, A., 2013. Ultrafast approximation for phylogenetic bootstrap. Mol. Biol. Evol. 30, 1188–1195. https://doi.org/10.1093/molbev/mst024.
Minh, B.Q., Schmidt, H.A., Chernomor, O., Schrempf, D., Woodhams, M.D., von Haeseler, A., Lanfear, R., 2020. IQ-TREE 2: new models and efficient methods for phylogenetic inference in the genomic era. Mol. Biol. Evol. 37, 1530–1534. https://doi.org/10.1093/molbev/msaa015.
Moghadasi, S.A., Biswas, R.G., Harki, D.A., Harris, R.S., 2023a. Rapid resistance profiling of SARS-CoV-2 protease inhibitors. npj Antimicrob Resist 1, 1–4. https://doi.org/10.1038/s44259-023-00009-0.
Moghadasi, S.A., Heilmann, E., Khalil, A.M., Nnabuife, C., Kearns, F.L., Ye, C., Moraes, S. N., Costacurta, F., Esler, M.A., Aihara, H., Harris, R.S., 2023b. Transmissible SARS-CoV-2 variants with resistance to clinical protease inhibitors. Sci. Adv. 9, eade8778 https://doi.org/10.1126/sciadv.ade8778.
Noske, G.D., Silva, E. de S., Godoy, M.O. de, Dolci, I., Fernandes, R.S., Guido, R.V.C., Sjö, P., Oliva, G., Godoy, A.S., 2023. Structural basis of nirmatrelvir and ensitrelvir activity against naturally occurring polymorphisms of the SARS-CoV-2 main protease. J. Biol. Chem. 299 https://doi.org/10.1016/j.jbc.2023.103004.
Owen, D.R., Allerton, C.M.N., Anderson, A.S., Aschenbrenner, L., Avery, M., Berritt, S., Boras, B., Cardin, R.D., Carlo, A., Coffman, K.J., Dantonio, A., Di, L., Eng, H., Ferre, R., Gajiwala, K.S., Gibson, S.A., Greasley, S.E., Hurst, B.L., Kadar, E.P., Kalgutkar, A.S., Lee, J.C., Lee, J., Liu, W., Mason, S.W., Noell, S., Novak, J.J., Obach, R.S., Ogilvie, K., Patel, N.C., Pettersson, M., Rai, D.K., Reese, M.R., Sammons, M.F., Sathish, J.G., Singh, R.S.P., Steppan, C.M., Stewart, A.E., Tuttle, J. B., Updyke, L., Verhoest, P.R., Wei, L., Yang, Q., Zhu, Y., 2021. An oral SARS-CoV-2 Mpro inhibitor clinical candidate for the treatment of COVID-19. Science 374, 1586–1593. https://doi.org/10.1126/science.abl4784.
O'Toole, Á., Scher, E., Underwood, A., Jackson, B., Hill, V., McCrone, J.T., Colquhoun, R., Ruis, C., Abu-Dahab, K., Taylor, B., Yeats, C., du Plessis, L., Maloney, D., Medd, N., Attwood, S.W., Aanensen, D.M., Holmes, E.C., Pybus, O.G., Rambaut, A., 2021. Assignment of epidemiological lineages in an emerging pandemic using the pangolin tool. Virus Evol 7, veab064. https://doi.org/10.1093/ve/veab064.
Pinto, D., Park, Y.-J., Beltramello, M., Walls, A.C., Tortorici, M.A., Bianchi, S., Jaconi, S., Culap, K., Zatta, F., De Marco, A., Peter, A., Guarino, B., Spreafico, R., Cameroni, E., Case, J.B., Chen, R.E., Havenar-Daughton, C., Snell, G., Telenti, A., Virgin, H.W., Lanzavecchia, A., Diamond, M.S., Fink, K., Veesler, D., Corti, D., 2020. Cross-neutralization of SARS-CoV-2 by a human monoclonal SARS-CoV antibody. Nature 583, 290–295. https://doi.org/10.1038/s41586-020-2349-y.
REED, L.J., MUENCH, H., 1938. A simple method of estimating fifty per cent ENDPOINTS12. Am. J. Epidemiol. 27, 493–497. https://doi.org/10.1093/oxfordjournals.aje.a118408.
Rockett, R., Basile, K., Maddocks, S., Fong, W., Agius, J.E., Johnson-Mackinnon, J., Arnott, A., Chandra, S., Gall, M., Draper, J., Martinez, E., Sim, E.M., Lee, C., Ngo, C., Ramsperger, M., Ginn, A.N., Wang, Q., Fennell, M., Ko, D., Lim, H.L., Gilroy, N., O'Sullivan, M.V.N., Chen, S.C.-A., Kok, J., Dwyer, D.E., Sintchenko, V., 2022. Resistance mutations in SARS-CoV-2 Delta variant after sotrovimab use. N. Engl. J. Med. 386, 1477–1479. https://doi.org/10.1056/NEJMc2120219.
Tracking SARS-CoV-2 variants [WWW Document]. n.d. https://www.who.int/activities/tracking-SARS-CoV-2-variants, 11.14.23.
Sasaki, M., Tabata, K., Kishimoto, M., Itakura, Y., Kobayashi, H., Ariizumi, T., Uemura, K., Toba, S., Kusakabe, S., Maruyama, Y., Iida, S., Nakajima, N., Suzuki, T., Yoshida, S., Nobori, H., Sanaki, T., Kato, T., Shishido, T., Hall, W.W., Orba, Y., Sato, A., Sawa, H., 2022. S-217622, a SARS-CoV-2 main protease inhibitor, decreases viral load and ameliorates COVID-19 severity in hamsters. Sci. Transl. Med. 15, eabq4064. https://doi.org/10.1126/scitranslmed.abq4064.
Shionogi, 2023. A Phase 3, Multicenter, Randomized, Double-Blind, 24-Week Study of the Clinical and Antiviral Effect of S-217622 Compared with Placebo in Non-hospitalized Participants with COVID-19 (Clinical Trial Registration No. NCT05305547). clinicaltrials.Gov.
Starr, T.N., Czudnochowski, N., Liu, Z., Zatta, F., Park, Y.-J., Addetia, A., Pinto, D., Beltramello, M., Hernandez, P., Greaney, A.J., Marzi, R., Glass, W.G., Zhang, I., Dingens, A.S., Bowen, J.E., Tortorici, M.A., Walls, A.C., Wojcechowskyj, J.A., De Marco, A., Rosen, L.E., Zhou, J., Montiel-Ruiz, M., Kaiser, H., Dillen, J.R., Tucker, H., Bassi, J., Silacci-Fregni, C., Housley, M.P., di Iulio, J., Lombardo, G., Agostini, M., Sprugasci, N., Culap, K., Jaconi, S., Meury, M., Dellota Jr., E., Abdelnabi, R., Foo, S.-Y.C., Cameroni, E., Stumpf, S., Croll, T.I., Nix, J.C., Havenar-Daughton, C., Piccoli, L., Benigni, F., Neyts, J., Telenti, A., Lempp, F.A., Pizzuto, M.S., Chodera, J. D., Hebner, C.M., Virgin, H.W., Whelan, S.P.J., Veesler, D., Corti, D., Bloom, J.D., Snell, G., 2021. SARS-CoV-2 RBD antibodies that maximize breadth and resistance to escape. Nature 597, 97–102. https://doi.org/10.1038/s41586-021-03807-6.
Takashita, E., Kinoshita, N., Yamayoshi, S., Sakai-Tagawa, Y., Fujisaki, S., Ito, M., Iwatsuki-Horimoto, K., Halfmann, P., Watanabe, S., Maeda, K., Imai, M., Mitsuya, H., Ohmagari, N., Takeda, M., Hasegawa, H., Kawaoka, Y., 2022. Efficacy of antiviral agents against the SARS-CoV-2 omicron subvariant BA.2. N. Engl. J. Med. 386, 1475–1477. https://doi.org/10.1056/NEJMc2201933.
Touret, F., Baronti, C., Goethals, O., Van Loock, M., de Lamballerie, X., Querat, G., 2019. Phylogenetically based establishment of a dengue virus panel, representing all available genotypes, as a tool in dengue drug discovery. Antivir. Res. 168, 109–113. https://doi.org/10.1016/j.antiviral.2019.05.005.
Touret, F., Gilles, M., Barral, K., Nougairède, A., van Helden, J., Decroly, E., de Lamballerie, X., Coutard, B., 2020. In vitro screening of a FDA approved chemical library reveals potential inhibitors of SARS-CoV-2 replication. Sci. Rep. 10 (13093) https://doi.org/10.1038/s41598-020-70143-6.
Touret, F., Driouich, J.-S., Cochin, M., Petit, P.R., Gilles, M., Barthélémy, K., Moureau, G., Mahon, F.-X., Malvy, D., Solas, C., de Lamballerie, X., Nougairède, A., 2021a. Preclinical evaluation of Imatinib does not support its use as an antiviral drug against SARS-CoV-2. Antivir. Res. 193 (105137) https://doi.org/10.1016/j.antiviral.2021.105137.
Touret, F., Driouich, J.-S., Cochin, M., Petit, P.R., Gilles, M., Barthélémy, K., Moureau, G., Mahon, F.-X., Malvy, D., Solas, C., de Lamballerie, X., Nougairède, A., 2021b. Preclinical evaluation of Imatinib does not support its use as an antiviral drug against SARS-CoV-2. Antivir. Res. 193 (105137) https://doi.org/10.1016/j.antiviral.2021.105137.
Touret, F., Baronti, C., Bouzidi, H.S., de Lamballerie, X., 2022. In vitro evaluation of therapeutic antibodies against a SARS-CoV-2 Omicron B.1.1.529 isolate. Sci. Rep. 12 (4683) https://doi.org/10.1038/s41598-022-08559-5.
Touret, F., Giraud, E., Bourret, J., Donati, F., Tran-Rajau, J., Chiaravalli, J., Lemoine, F., Agou, F., Simon-Lorière, E., van der Werf, S., de Lamballerie, X., 2023. Enhanced neutralization escape to therapeutic monoclonal antibodies by SARS-CoV-2 omicron sub-lineages. iScience 26 (106413). https://doi.org/10.1016/j.isci.2023.106413.
University of Minnesota, 2023. Strategies and Treatments for Respiratory Infections & Viral Emergencies (STRIVE): Shionogi Protease Inhibitor (Clinical Trial Registration No. NCT05605093). clinicaltrials.Gov.
Unoh, Y., Uehara, S., Nakahara, K., Nobori, H., Yamatsu, Y., Yamamoto, S., Maruyama, Y., Taoda, Y., Kasamatsu, K., Suto, T., Kouki, K., Nakahashi, A., Kawashima, S., Sanaki, T., Toba, S., Uemura, K., Mizutare, T., Ando, S., Sasaki, M., Orba, Y., Sawa, H., Sato, A., Sato, T., Kato, T., Tachibana, Y., 2022. Discovery of S-217622, a noncovalent oral SARS-CoV-2 3CL protease inhibitor clinical candidate for treating COVID-19. J. Med. Chem. 65, 6499–6512. https://doi.org/10.1021/acs.jmedchem.2c00117.
Vangeel, L., Chiu, W., De Jonghe, S., Maes, P., Slechten, B., Raymenants, J., André, E., Leyssen, P., Neyts, J., Jochmans, D., 2022. Remdesivir, Molnupiravir and Nirmatrelvir remain active against SARS-CoV-2 Omicron and other variants of concern. Antivir. Res. 198 (105252) https://doi.org/10.1016/j.antiviral.2022.105252.
Wang, M., Cao, R., Zhang, L., Yang, X., Liu, J., Xu, M., Shi, Z., Hu, Z., Zhong, W., Xiao, G., 2020. Remdesivir and chloroquine effectively inhibit the recently emerged novel coronavirus (2019-nCoV) in vitro. Cell Res. 1–3. https://doi.org/10.1038/s41422-020-0282-0.
Williamson, B.N., Feldmann, F., Schwarz, B., Meade-White, K., Porter, D.P., Schulz, J., van Doremalen, N., Leighton, I., Yinda, C.K., Pérez-Pérez, L., Okumura, A., Lovaglio, J., Hanley, P.W., Saturday, G., Bosio, C.M., Anzick, S., Barbian, K., Cihlar, T., Martens, C., Scott, D.P., Munster, V.J., de Wit, E., 2020. Clinical benefit of remdesivir in rhesus macaques infected with SARS-CoV-2. Nature 585, 273–276. https://doi.org/10.1038/s41586-020-2423-5.
Xocova Filed for Conditional Approval in South Korea [WWW Document]. Pharma Japan. n.d. https://pj.jiho.jp/article/248085, 11.14.23.
Xocova to Be Commercially. Pharma Japan. Available from March 31 [WWW Document], n.d. https://pj.jiho.jp/article/248538, 10.31.23.